Report Documentation Page		Form Approved OMB No. 0704-0188

Public reporting burden for the collection of information is estimated to average 1 hour per response, including the time for reviewing instructions, searching existing data sources, gathering and maintaining the data needed, and completing and reviewing the collection of information. Send comments regarding this burden estimate or any other aspect of this collection of information, including suggestions for reducing this burden, to Washington Headquarters Services, Directorate for Information Operations and Reports, 1215 Jefferson Davis Highway, Suite 1204, Arlington VA 22202-4302. Respondents should be aware that notwithstanding any other provision of law, no person shall be subject to a penalty for failing to comply with a collection of information if it does not display a currently valid OMB control number.

1. REPORT DATE **APR 2011**	2. REPORT TYPE	3. DATES COVERED **00-00-2011 to 00-00-2011**
4. TITLE AND SUBTITLE **Off-Axis Detection and Characterization of Laser Beams in the Maritime Atmosphere**		5a. CONTRACT NUMBER
		5b. GRANT NUMBER
		5c. PROGRAM ELEMENT NUMBER
6. AUTHOR(S)		5d. PROJECT NUMBER
		5e. TASK NUMBER
		5f. WORK UNIT NUMBER
7. PERFORMING ORGANIZATION NAME(S) AND ADDRESS(ES) **Space and Naval Warfare Systems Center Pacific,San Diego,CA,92152**		8. PERFORMING ORGANIZATION REPORT NUMBER
9. SPONSORING/MONITORING AGENCY NAME(S) AND ADDRESS(ES)		10. SPONSOR/MONITOR'S ACRONYM(S)
		11. SPONSOR/MONITOR'S REPORT NUMBER(S)
12. DISTRIBUTION/AVAILABILITY STATEMENT **Approved for public release; distribution unlimited**		
13. SUPPLEMENTARY NOTES		
14. ABSTRACT		
15. SUBJECT TERMS		

16. SECURITY CLASSIFICATION OF:			17. LIMITATION OF ABSTRACT	18. NUMBER OF PAGES	19a. NAME OF RESPONSIBLE PERSON
a. REPORT **unclassified**	b. ABSTRACT **unclassified**	c. THIS PAGE **unclassified**	**Same as Report (SAR)**	**23**	

Standard Form 298 (Rev. 8-98)
Prescribed by ANSI Std Z39-18

Off-Axis Detection and Characterization of Laser Beams in the Maritime Atmosphere

Frank Hanson,[*] **Ike Bendall, Christina Deckard, and Hiba Haidar**
Space and Naval Warfare Systems Center Pacific
San Diego, CA 92152

[*] Corresponding author: *hansonfe@spawar.navy.mil*

Remote detection and characterization of laser beams propagating in maritime atmospheres is discussed. A model for off-axis scattered laser light based on Mie scattering from maritime aerosols is presented and compared with angle and time-resolved measurements from a pulsed laser source. We demonstrate that the direction of the source can be determined from the angle-resolved intensity and that the beam direction can be determined from arrival times of the scattered signals if the position of the laser source is known.

OCIS codes: 010.1310, 280.3420, 290.1310, 290.4210, 290.5825

1. Introduction

Free-space lasers are becoming more widely used in the military environment, and it is important to develop a capability to detect and remotely characterize laser beams from an off-axis location. Many applications in communication, surveillance and targeting, require relatively high-power or pulsed laser sources and involve propagation distances of several kilometers. If such lasers are used as a threat, it would be desirable to know the power and location of the source and the direction of the beam in order to provide warning and enable counter-measures. Previous work has demonstrated that pulsed laser beams can be detected from scattering by aerosols in the path and the beam can be imaged with suitable detectors [1]. There a 10x10 detector array was used and the scattered intensity was found to be roughly consistent with the prediction based on Mie scattering from a generic continental aerosol distribution. Aerosol concentrations can vary widely depending on regional and local weather conditions. More recent work has investigated how details of the aerosol distribution would affect the scattered intensity [2,3]. For example, increased humidity will lead to larger aerosols and generally enhance the scattering. In typical conditions, even at low altitude, the scattering is extremely weak and can be difficult to detect in the presence of background light.

In this work, we present a detailed theory of the remote detection of scattered light and make comparisons with Monte Carlo calculations to understand the effect of multiple scattering on the received intensity. Extensive experimental intensity and temporal data from a high-speed 30-channel angle-resolved receiver is presented and compared with the analytic theory. Volume scattering is estimated by using a range of modeled aerosol distributions representative of the observed weather conditions. The high angular resolution of the receiver allowed the direction of the source to be tracked as the geometry of the experiment evolved over time. Assuming a volume scattering function, the laser power and distance as well as the direction of the beam all affect the scattered intensity at the receiver and these parameters cannot be readily distinguished from intensity data alone. If the location of the source is know, there would still be an ambiguity between power and beam direction. In this case, we show that accurate timing information of the received scattered light can be used to estimate beam direction and subsequently laser power.

2. Off-Axis Scattering Theory

The scattering plane geometry is defined in Fig. 1. The receiver and laser source are separated by R and the beam from the source is oriented at an angle ψ from the baseline between them. At the size-scale of interest in this work it is a good approximation to neglect beam size and divergence and treat the beam as one-dimensional. The receiver collects scattered light from a laser pulse at an angle θ from the baseline corresponding to a propagation distance z along the beam line. The scattered light travels a distance r to the receiver. The angle from the direction of the source to a reference direction on the receiver is given by θ_s.

We consider the light collected by the receiver to be only due to volume scattering from aerosols in the path of the beam. The scattering is characterized by a volume scattering function $\beta(\psi+\theta)$ ($m^{-1}sr^{-1}$) which depends on the scattering angle $\psi+\theta$ from the direction of propagation. In general, the scattering will vary with position but for simplicity, we assume β to be spatially uniform. The laser power is extinguished along the beam line as $P_0\exp(-\alpha z)$ where α is the beam

2

extinction coefficient due to absorption a and total scattering $b = 2\pi \int_0^\pi \sin(\theta)\beta(\theta)d\theta$ along the path. We will neglect multiple scattering, which is a good approximation if the mean free path $1/b$ is large compared with the spatial scale of the experiments. If we assume a uniform homogeneous medium, the angle and time-dependent scattered radiance at the receiver from a laser pulse with an initial power $P_0(t)$ can be written in terms of the beam extinction coefficient α and the volume scattering function β as

$$\frac{dI(\theta,t)}{d\theta} = P_0\left[t_{SR}(\theta)-t\right]\exp\left[-\alpha(z+r)\right]\frac{\beta(\theta+\psi)}{r^2}\frac{dz}{d\theta}. \tag{1}$$

Here $z(\theta) = R\sin(\theta)/\sin(\theta+\psi)$ and $r(\theta) = R\sin(\psi)/\sin(\theta+\psi)$ are the distances from the scattering volume to the source and receiver respectively and $t_{SR}(\theta) = (z+r)/c$ is the propagation time along the path from the source to receiver. If a detector collects scattered light over a limited one-dimensional angular range $\Delta\theta$ in the scattering plane, the total intensity $I(\theta,t)$ centered at θ in the middle of the range $\Delta\theta$ will be a convolution of the time-dependent pulse with the scattering along the path subtended by $\Delta\theta$. After simplifying, this becomes

$$I(\theta,t) = \int_{\theta-\Delta\theta/2}^{\theta+\Delta\theta/2} P_0\left[t_{SR}(\theta')-t\right]\exp\left[-\alpha(z+r)\right]\frac{\beta(\theta'+\psi)}{R\sin(\psi)}d\theta'. \tag{2}$$

The peak intensity at the receiver is usually required and therefore it is necessary to determine the time t that maximizes $I(\theta,t)$. The propagation time increases with both ψ and θ and the variation of t_{SR} with θ is

$$\frac{dt_{SR}}{d\theta} = \frac{R}{2c}\sin(\psi)\Big/\cos\left[(\theta+\psi)/2\right]^2. \tag{3}$$

Some approximations that simplify Eq. 2 can often be made, depending on the variation of $P_0(t_{SR}(\theta)-t)$ and $\beta(\theta+\psi)$ over $\Delta\theta$ [1]. Consider the ratio $\tau/\Delta t_{SR}$ of laser pulse width τ to the range of t_{SR} over $\Delta\theta$. In the long-pulse limit where the ratio is large, the maximum intensity occurs at $t \approx t_{SR}(\theta)$ and $P_0(t_{SR}(\theta)-t) \approx P_0(0)$. As the ratio decreases and τ becomes comparable to or shorter than Δt_{SR}, the sensitivity of $I(\theta,t)$ with respect to t increases. The maximum intensity is found when the pulse is centered at angles nearer to the source because the scattering function β is generally larger for smaller scattering angles. In the analysis below, the integration (Eq. 2) was

replaced by an analytic summation over discrete angles within $\Delta\theta$, and the sum was maximized with respect to t as a parameter. A much simpler and often good approximation is to simply center the pulse at the midpoint of integration. For our experimental conditions (see below), we found this approximation to underestimate the maximum of $I(\theta,t)$ by less than ~10% for larger ψ and smaller θ where the error is greatest.

3. Experiment

Scattering data at $\lambda = 1.06$ μm was collected with the Ship Board Laser Acquisition System (SBLAS) [4], a high-speed multi-channel receiver that could record arrival time and intensity over a horizontal field of view (FOV) from -45º to +45º. The SBLAS was composed of two 15-element linear detector arrays with separate collection optics that covered the range, in receiver coordinates θ-θ_S, from -45º to 0º and from 0 to 45º respectively. The aperture normal and optical axis of each side was inclined to the middle of the respective 45º-range. Each of the 30 angular channels had a narrow asymmetric FOV, $\Delta\theta = 3º$ in the horizontal plane and $-15º < \theta_V < 15º$ in the vertical plane. Each channel digitized the signal and recorded the crossing time over 9 threshold values. Depending on the highest threshold crossed, the true peak intensity could exceed the threshold value by a factor of one to four. The experiments described below were conducted in full daylight conditions in the presence of significant background radiance. However, the detectors were AC-coupled and the constant background had little effect. False alarms in the receiver were further reduced by requiring a valid detection event to consist of responses in multiple channels with timing consistent with the propagation of a laser pulse.

Beam scattering experiments were performed over several days off the coast of Cowley beach, Queensland Australia. A laser source ($\lambda = 1.06$ μm) with pulse width $\tau = 20$ ns full width at half maximum was located on the beach about 1-2 m above sea level and the beam was collimated and directed at a stationary target boat offshore. The SBLAS receiver was mounted on another ship with its axis facing to starboard and perpendicular to the heading of the ship. The extensive experimental data taken on 1 July 2004 exemplifies the capability of the receiver over a significant variation of scattering geometry and allows a meaningful comparison with the theoretical model discussed above. GPS positioning data taken on the ship allowed the path of the receiver relative to the laser beam to be reconstructed as shown in Fig. 2. During this experiment the ship followed a path ~ 4.8 km from shore and approximately perpendicular to the laser beam.

As mentioned earlier, atmospheric aerosols in the beam path are the source of off-axis laser scatter. Some limited measurements of the aerosol size distribution at the ship were made however they were not considered to be of sufficient quality to predict the volume scattering accurately. Furthermore, over the beam path that extended nearly 5 km from the shore, the aerosol distribution was unlikely to be uniform. Fortunately there has been significant effort devoted to developing models that describe the generation and distribution of aerosols in maritime environments based on environmental conditions [5,6,7]. Here we have used the Advanced Navy Aerosol Model (ANAM) [7] to predict representative aerosol distributions consistent with the weather conditions preceding and during the experiment. ANAM includes five distinct types of uniform spherical particles, each with a log-normal distribution based on radius. Details of the model are described in the appendix. Over open water, the current wind speed and the preceding 24-hour average wind speed are perhaps the most significant factors in

the production of aqueous aerosols, especially the larger aerosols that lead disproportionally to small-angle forward scattering.

Measurements of wind speed w, temperature T and relative humidity RH were continuously recorded on the ship beginning at 9:00 AM local time. The collection of scattering data began at approximately 2 PM and lasted for ~280 seconds while the ship followed the path shown in Fig. 2. During this period the wind speed varied between 2 and 8 m/s and the average wind speed over 5 hours preceding the test was ~3 m/s. It is important to note that these conditions were measured some kilometers from the beam scattering and were probably not uniform over the entire region. Therefore we used ANAM to generate four representative aerosol distributions that should have bracketed the range of scattering conditions during the tests. The environmental parameters used in the four cases are given in Table 1. The largest and heaviest aerosols with modal radius ~10 µm are generated by wind action on the sea surface and the equilibrium density decreases quickly with height h. They are expected to be significant near the sea surface at $h = 2$ m. For comparison, a case with $h = 300$ m was chosen to effectively eliminate these aerosols which were not present in the earlier NAM aerosol model [5]. The air-mass parameter (amp) is meant to describe the relative coastal influence (from 0 to 10) and lacking specific information, we chose cases with $amp = 3$ (less coastal influence) and $amp = 8$ (more influence).

The ANAM model includes wavelength-dependent absorption and refractive indices for the spherical aerosols. For each of the four cases, the Bohren-Huffman MIE scattering code [8] was used to calculate the angle-dependent volume scattering function appropriate for detection of scattered light from a source polarized perpendicular to the scattering plane, $\beta = (\lambda/2\pi)^2 (S_{11} - S_{12})$, where S_{ij} are Mueller matrix elements. These representative scattering functions for $\lambda = 1.06$ µm are compared in Fig. 3. Some notable features are apparent. First, there is a pronounced decrease in small-angle forward scattering for the aerosols of Case 3 that do not include the largest radius aerosols centered near 10 µm. Case 4 differs from Case 2 only by a larger air-mass parameter and consequently the inclusion of the small, high refractive index, dust-like aerosols that lead to an increase in scattering above about 3º. The total beam extinction ($a+b$) varied over a factor of ~5 for these cases. Measurements of the laser beam extinction would have been useful to help characterize the aerosol conditions during the experiments but were not taken.

Next we compare the model predictions with the data from the SBLAS receiver during the experiment off Cowley Beach, Australia. GPS position data taken on the ship were recorded along with the receiver data at a rate of 10 readings per second and were precise to about 2 m and 5 m along the east-west (x) and south-north (y) directions respectively. A piece-wise linear fit of the GPS coordinates, in segments of 15 seconds, was used to construct the ship heading from which the source angle θ_S or orientation of the receiver relative to the source-receiver baseline and beam angle ψ were calculated. In Fig. 4 we show how θ_S fluctuated 2-3º during the experiment due to variations of the heading from a straight path. However the beam angle ψ, because it is defined relative to the position (rather than orientation) of the receiver, was insensitive to the small heading fluctuations. An estimate of the source angle θ_{SE} was obtained from the intensity data by taking the angle of the channel with the largest signal. Since the direction of the beam to the left or right was always apparent, ambiguities among multiple channels recording the same intensity threshold were resolved by selecting the channel nearest the source. Although θ_{SE} was only resolved to 3º, these measurements are clearly correlated with the GPS tracking data.

5

Scattering data from the SBLAS receiver was recorded for each firing of the laser and 2742 measurements were collected as the receiver traversed the beam line. The SBLAS signal was corrected to give intensity (W/m^2) in the direction of receiver coordinate θ - θ_S and normalized to the peak power of the laser pulse, assuming a Gaussian temporal profile with pulse width τ = 20 ns full width at half maximum. Six measurements from discrete laser firings at selected beam angles ψ in the range from -6.5° to +6.5° are shown in Figs. 5 and 6. The data generally lie within the range of predictions of the scattering model (Eq. 2) using the volume scattering functions associated with the four aerosol cases. In particular, the data show essentially the same exponential decrease of intensity with angle over most of the angle range. At small scattering angles $\theta+\psi$, less than about 2°, the model predicts a large enhancement because of the increase of both $\beta(\theta+\psi)$ and dz/dθ (Eq. 1). This is especially pronounced when the largest aerosols are present and contribute to the small-angle volume scattering in cases 1,2 and 4. Some evidence of a slight enhancement in the data was seen for $|\psi| < $ ~1° but generally the measurements do not show the same magnitude of small-angle scattering, perhaps in part because fewer large aerosols were actually present in the beam path.

Although the single-scattering model gives quite good agreement with the measured intensity, it is important to understand how much the accuracy is affected by the neglect of multiple scattering. Since each angular channel within the SBLAS receiver has a large asymmetric FOV, some multiple scattering especially from laser power scattered close to the beam line, will be detected and lead to a larger signal than predicted. In order to verify the model we have performed a Monte Carlo (MC) simulation for a geometry similar to the experiment using the volume scattering function of Case 4 which has the largest beam extinction (~16%/km). The MC procedure has been described in previous work [9]. In this simulation 10^8 photons were launched along a beam line normal to a collection plane located d = 4778 meters away. The normalized scattered intensity (m^{-2}) for a desired beam angle ψ was obtained from the fraction collected in an annular ring with center radius $x = d \tan(\psi)$ and width Δx = 5 m and then resolved into angular channels $\Delta\theta$ = 3°. A scattering plane for each photon was defined by the beam line and the impact point in the annulus which then allowed the out-of-plane angle of incidence to be calculated. Although the SBLAS receiver had a symmetric vertical FOV, the proximity of the ocean surface to the beam and receiver meant that the effective vertical FOV was reduced to 0 δ θ_V <15° and therefore only photons collected within this FOV were counted. Figure 7 compares normalized receiver intensities (W/m^2/W) for beam angles ψ = 0.6°, 2.4° and 9.5° (θ_S = -ψ) with the model prediction where the laser power P_0 was constant. Both the model and the MC results show the enhanced receiver intensity at small scattering angles $\theta+\psi$ and the nearly exponentially decrease at larger angles. As expected, the single-scatter model somewhat underestimates the intensity when the beam is in the receiver FOV. The MC results also show weak intensity at angles behind the beam due to multiple scattering that is not accounted for in the model. When only singly-scattered photons were counted, the MC results were consistent with the model. When the beam was in the receiver FOV, the relative difference increases with larger beam angles because each channel FOV encompasses a larger volume of space from which multiply scattered light originates. At ψ = 9.5° the difference is ~15%, however, including scattering from a symmetric FOV -15° < θ_V <15° would have doubled this.

One would like to characterize the power and location of the laser source as well as the direction of the beam from the receiver data and the model above. For many conditions, including those of this experiment, the analytic model provides a good approximation to the

scattered intensity observed remotely. However, assuming that the volume scattering can be estimated accurately, these three parameters cannot be determined unambiguously from the receiver intensity alone (Eq. 2). Two or more spatially separated receivers could be used to locate the direction and distance to the laser source by triangulation and, in this case, the relative intensity could then be used to resolve the ambiguity between laser power and beam direction. Here we demonstrate that, with a single receiver, the beam angle ψ can be determined from timing measurements of the scattered light if the position of the source is known. Then, with this information, the laser power can be estimated.

The SBLAS receiver recorded the relative times if and when each of the level thresholds was crossed for each receiver angle. We considered the crossing of the highest threshold t_H to approximate the time of peak intensity and representative timing data t_H over the receiver angles with some detected signal for selected beam angles ψ are shown in Fig. 8. The analytic path time $t_{SR} - t_0 = (z+r)/c - t_0$, based on the known geometry, matches this data with an offset time t_0 obtained by a least squares linear fitting procedure. Here, the variation of t_{SR} with angle is essentially linear. There is less than 1% variation between $dt_{SR}/d\theta$ calculated at $<\theta>$ and $<dt_{SR}/d\theta>$ averaged over θ. For each laser shot, the experimental average time derivative $<dt_H/d\theta>$ was calculated from a linear fit of t_H over angle. These measured values agreed well with the predicted derivative (Eq. 3), with θ evaluated at the mid-point.

The beam angle ψ can be determined from $dt_{SR}/d\theta$ using Eq. 3 if the source angle θ_S and range R are known. For each of the 2742 measurements, an estimate of ψ was calculated by substituting $<dt_H/d\theta>$ on the left hand side of Eq. 3 and solving for ψ using the estimated source angle θ_{SE} and known range R (from GPS data). Figure 9 shows the difference between the calculated beam angle ψ_c and the angle from the GPS tracking data. Over the range from -6° to +6° the rms error is 0.22°. The laser power can then be calculated from Eq. 2 based on an estimate of the beam extinction.

4. Conclusion

The remote detection of pulsed laser beams by scattering from atmospheric aerosols has been investigated. A theory of the angle and time-dependent scattered intensity for a general configuration of laser source, receiver and beam direction has been described. We have presented extensive measurements of off-axis scattering observed at ranges up to ~5 km with a high-speed multi-channel receiver. A beam of 20-ns laser pulses from a fixed laser source was propagated above the sea surface and detected by a multichannel receiver on a ship that traveled across the beam line. The high angular resolution of the receiver allowed the direction of the source to be tracked during the experiment. Representative aerosol distributions were calculated with the Advanced Navy Aerosol Model for the range of observed weather conditions and Mie theory was used to predict intensity at the receiver. The laser beam scattering was predominately in the forward direction and receiver intensity depended critically on the beam angle relative to the baseline between source and receiver. The scattering model gave reasonably good agreement with experiment, within the uncertainty of the aerosol conditions, up to beam angles $|\psi| < ~6.5°$ where the scattering was sufficiently strong for the SBLAS receiver. The receiver also recorded the relative arrival times of the scattered light for each of the angular channels. The change in arrival time with angle, along with information about the source position, was used to calculate the beam angle ψ.

Appendix

The Advanced Navy Aerosol Model (ANAM) is based on several years of work to predict the aerosol distribution in a maritime environment [5,7]. Here, the aerosols are considered to be uniform spherical particles with radius r and refractive index n. ANAM includes five distinct types of aerosol particles each characterized by a log-normal distribution peaked at a humidity-dependent modal radius ρ_s

$$\frac{dN}{dr} = \sum_{i=0}^{4} \frac{N_i}{\sqrt{2\pi}\sigma_i \exp\left(\sigma_i^2/2\right)\rho_{si}} \exp\left\{-\frac{\left[\ln\left(r/\rho_{si}\right)\right]^2}{2\sigma_i^2}\right\},$$

(A1)

with a width parameter $\sigma_i = 1/2^{1/2}$ ($i = 0,3$) and $\sigma_4 = 1/2$. Particle 0 is a non-hygroscopic dust particle originating over land with modal radius $\rho_s = \rho_0$. For all other particles, the modal radii increase with the fractional relative humidity s (0 to 1) according to $\rho_s = g(s)\rho_0$ with $g(s) = [(A-s)/B(1-s)]^{1/3}$. Similarly, the complex refractive indices for particles 1-4 are volume-weighted averages $n = n_W + (n_0 - n_W)g^3(0)/g^3(s)$, where n_0 is the index of the dry particle material and n_W is the index of water ($n_W = 1.326 + i\,4.83 \times 10^{-6}$ at $\lambda = 1.06$ µm). Values of these parameters are given in Table A1. In this implementation of ANAM, the total number density N_i (cm^{-3}) of each particle type depends on the air-mass parameter (amp), wind speed w (m/s) 24-hour average wind speed W (m/s), and height h (m) above the sea surface,

$$\left.\begin{cases} N_0 = 0 \\ N_1 = 136.55\,amp^2 \end{cases}\right\} \quad amp \leq 5$$

(A2)

$$\left.\begin{cases} N_0 = 0.3 \times 136.55\,amp^2 \\ N_1 = 0.7 \times 136.55\,amp^2 \end{cases}\right\} \quad amp > 5$$

(A3)

$$N_2 = 0.5462\,Max\left[5.866(W-2.2), 0.5\right],$$

(A4)

$$N_3 = 0.007214 \times 10^{\wedge}(0.06w),$$

(A5)

$$N_4 = 0.01x10^{\wedge}(0.07w - 0.04h).$$

(A6)

Acknowledgment

References

1. J. P. Cariou, "Off-axis detection of pulsed laser beams: simulation and measurements in the lower atmosphere," Proc. SPIE **5086**, 129-138 (2003).

2. N. Roy and F. Reid, "Off-axis laser detection model in coastal areas," Opt. Eng. **47**, 1-11 (2008).

3. J. K. Michulec and R. Schleijpen, "Influence of aerosols on off-axis laser detection capabilities," Proc. SPIE 7463, 1-12 (2009).

4. The SBLAS receiver was manufactured by the Goodrich Corp., Danbury, CT.

5. S. G. Gathman, ''Optical properties of the marine aerosol as predicted by the Navy aerosol model,'' *Opt. Eng.* **22**, 57–62 (1983).

6. J. Piazzola and G. Kaloshin, "Performance evaluation of the coastal aerosol extinction code MEDEX with data from the Black Sea," J. Aerosol Sci. **36**, 341-359 (2005).

7. S. Hammel, A. van Eijk, D. Tsintikidis, "ANAM vs. NAM: is the difference significant?" Proc. SPIE **5891**, 1-12 (2005).

8. C. F. Bohren and D. R. Huffman, *Absorption and Scattering of Light by Small Particles*, Wiley-Interscience, New York (1983).

9. F. Hanson and S. Radic, "High bandwidth underwater optical communication," Appl. Opt. **47**, 277-283 (2008).

FIGURE CAPTIONS

Figure 1. In this off-axis scattering geometry the laser and receiver are separated by R along the baseline between them. The laser beam is at an angle ψ to the baseline. Scattered light is detected by the receiver at an angle θ corresponding to a distance z along the beam line from the source and travels a distance r to the receiver. θ_S is the angle to a reference direction on the receiver.

Figure 2. The laser source is located just on shore at Cowley Beach, Queensland, Australia and the path of the receiver was nearly parallel to shore and perpendicular to the beam (red). The horizontal receiver FOV, shown schematically at one point on the path, was centered directly to starboard.

Figure 3. Volume scattering functions calculated from the ANAM cases in Table 1. The scattering angle relative to the beam direction is $\theta + \psi$.

Figure 4. An estimate of the (negative) source angle $-\theta_{SE}$ obtained from the SBLAS sensor (blue circles) is compared with the (negative) source angle $-\theta_S$ (black) and beam angle ψ (dashed) derived from the GPS tracking data.

Figure 5. Normalized scattered intensity at the receiver for three selected points along the ship path prior to crossing the beam line. The model predictions are calculated on a 0.5º grid with $\Delta\theta$ = 3.0º, for the four aerosol cases of Table 1. The receiver orientations relative to the source θ_S and the beam angles ψ were taken from GPS tracking data.

Figure 6. Normalized scattered intensity at the receiver for three selected points along the ship path after crossing the beam line. The model predictions are calculated as in Fig. 5.

Figure 7. Comparison of the single-scatter model (black line) and Monte Carlo calculations (10^8 photons) for the experimental geometry and beam angles $\psi = 0.6º$ (O), $2.4º$ (□) and $9.5º$ (△) and the aerosol scattering function from Case 4. The MC results show slightly greater scattering than the model prediction due to multiple scattering and also scattering from behind the beam line.

Figure 8. The relative propagation time from the laser to the receiver determined by the crossing time of the highest threshold level for single measurements at beam angles $\psi = -6.0º$ (●), $-1.5º$ (■), $1.5º$ (◆), and $6.0º$ (▲). Timing curves calculated from $(z+r)/c$ using the known geometry and offset to give the best fit are shown as dashed lines.

Figure 9. Difference of beam angle ψ_c (blue) calculated from Eq. 3 using the estimated source angle θ_{SE} and timing data $<dt_H/d\theta>$ from SBLAS and the beam angle obtained from GPS data.
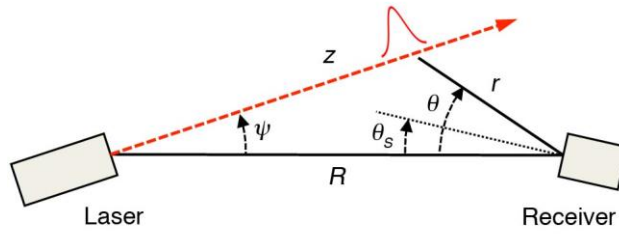
Fig. 1. In this off-axis scattering geometry the laser and receiver are separated by R along the baseline between them. The laser beam is at an angle ψ to the baseline. Scattered light is detected by the receiver at an angle θ corresponding to a distance z along the beam line from the source and travels a distance r to the receiver. θ_S is the angle to a reference direction on the receiver.
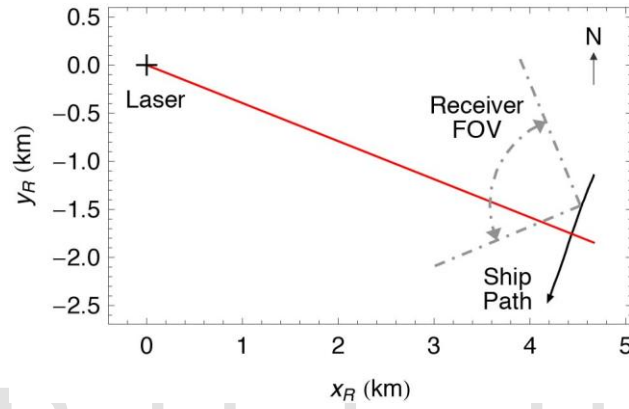
Fig. 2. The laser source is located just on shore at Cowley Beach, Queensland, Australia and the path of the receiver was nearly parallel to shore and perpendicular to the beam (red). The horizontal receiver FOV, shown schematically at one point on the path, was centered directly to starboard.
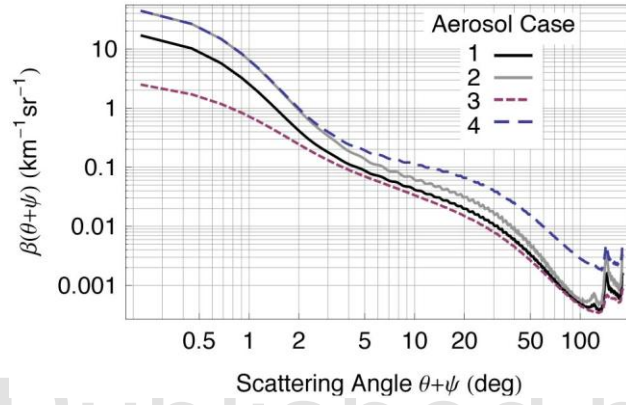
Fig. 3. Volume scattering functions calculated from the ANAM cases in Table 1. The scattering angle relative to the beam direction is $\theta + \psi$.
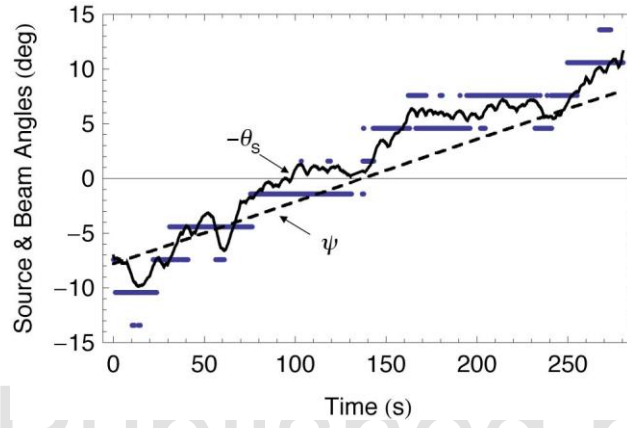
Fig. 4. An estimate of the (negative) source angle $-\theta_{SE}$ obtained from the SBLAS sensor (blue circles) is compared with the (negative) source angle $-\theta_S$ (black) and beam angle ψ (dashed) derived from the GPS tracking data.
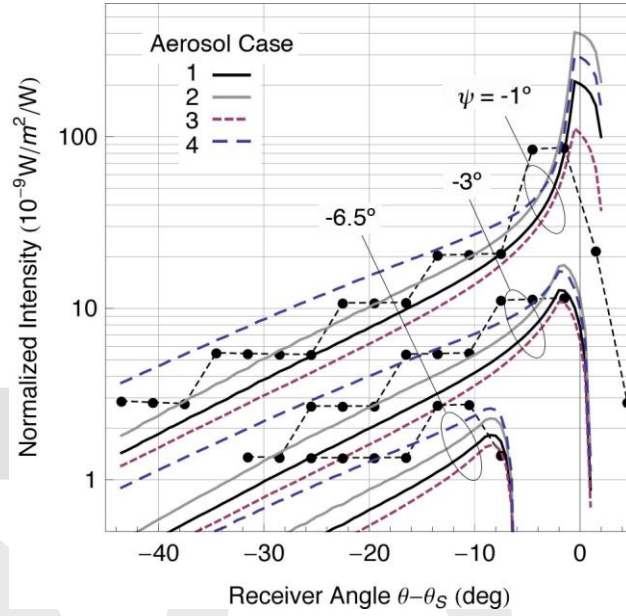
Fig. 5. Normalized scattered intensity at the receiver for three selected points along the ship path prior to crossing the beam line. The model predictions are calculated on a 0.5° grid with $\Delta\theta = 3.0°$, for the four aerosol cases of Table 1. The receiver orientations relative to the source θ_S and the beam angles ψ were taken from GPS tracking data.
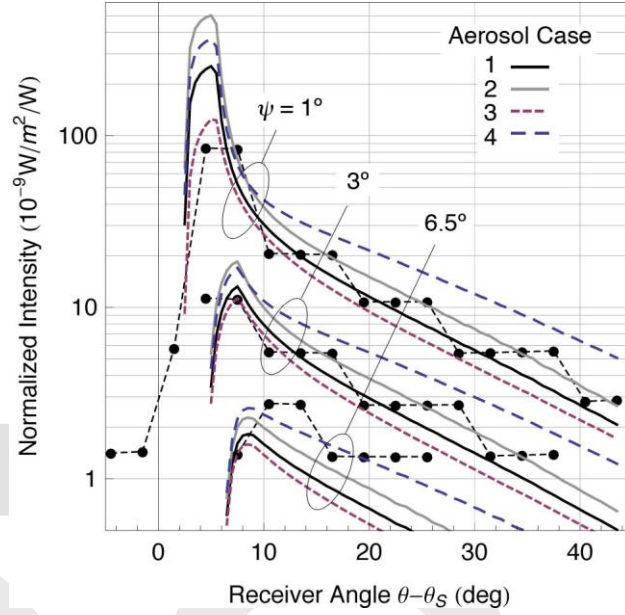
Fig. 6. Normalized scattered intensity at the receiver for three selected points along the ship path after crossing the beam line. The model predictions are calculated as in Fig. 5.
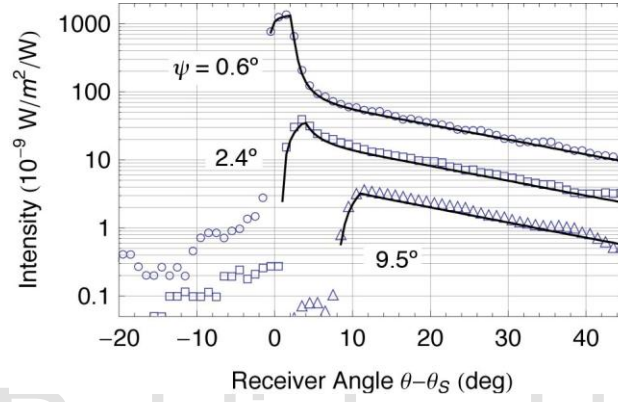
Fig. 7. Comparison of the single-scatter model (black line) and Monte Carlo calculations (10^8 photons) for the experimental geometry and beam angles $\psi = 0.6º$ (○), 2.4º (□) and 9.5º (△) and the aerosol scattering function from Case 4. The MC results show slightly greater scattering than the model prediction due to multiple scattering and also scattering from behind the beam line.
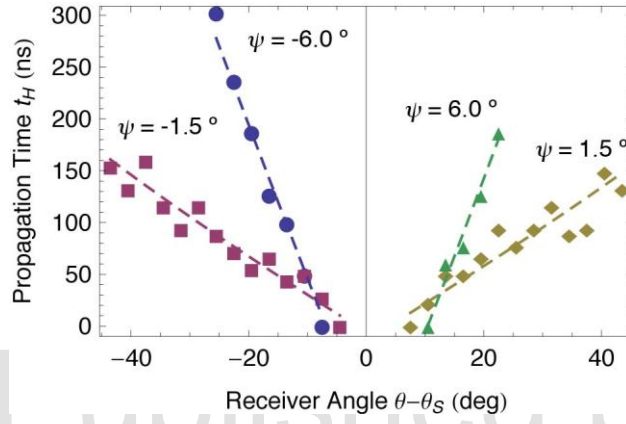
Fig. 8. The relative propagation time from the laser to the receiver determined by the crossing time of the highest threshold level for single measurements at beam angles ψ = -6.0º ($\bullet$), -1.5º ($\blacksquare$), 1.5º ($\blacklozenge$), and 6.0º ($\blacktriangle$). Timing curves calculated from $(z+r)/c$ using the known geometry and offset to give the best fit are shown as dashed lines.

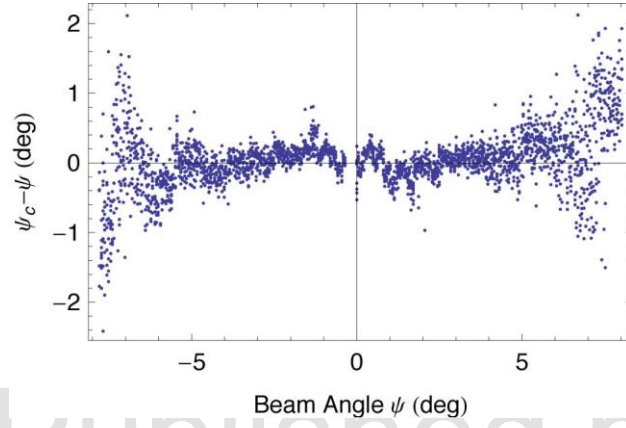Fig. 9. Difference of beam angle ψ_c (blue) calculated from Eq. 3 using the estimated source angle θ_{SE} and timing data $<\mathrm{d}t_H/\mathrm{d}\theta>$ from SBLAS and the beam angle obtained from GPS data.

Table 1. ANAM environmental parameters used to generate the four aerosol distributions and the total scattering coefficient *b* and absorption coefficient *a* calculated from the MIE code.

Aerosol Case	Wind Speed w (m/s)	*amp*	Height h (m)	b (km^{-1})	a (km^{-1})
1	2	3	2	0.0474	0.00023
2	8	3	2	0.0828	0.00058
3	8	3	300	0.0316	0.00006
4	8	8	2	0.1563	0.00219

In all cases, the relative humidity was 90% and the 24-hour average wind speed was 3 m/s.

Table A1. ANAM parameters for each of the 5 particle types.

Particle	ρ_0 (μm)	n_0 ($\lambda = 1.06$ μm)	A	B
0	0.03	$1.52 + i\ 0.008$	-	-
1	0.03	$1.392 + i\ 0.000153$	1.17	1.87
2	0.24	$1.47 + i\ 0.0002$	1.83	5.13
3	2.0	$1.47 + i\ 0.0002$	1.97	5.83
4	8.0	$1.47 + i\ 0.0002$	1.97	5.83